Appl. Comput. Math., V.22, N.3, Special Issue, 2023, pp.317-337
DOI: 10.30546/1683-6154.22.3.2023.317

A QUARTIC NONLINEAR FLUX-CONTROLLED MEMRISTOR MODEL AND ITS APPLICATION IN CHAOTIC SYSTEM

YANJIE MA[1], JUN MOU[1,*], SANTO BANERJEE[2], MIAO MIAO[1,*]

Abstract. In this paper, a novel model of the flux-controlled memristor is constructed and the characteristics of the model are analyzed. After that, a memristive chaotic system based on this memristor is constructed and its dynamical behavior is analyzed, and the attractor coexistence and state transfer phenomena are observed. In addition, the equivalent circuits of the memristor model and the system are designed, and the system is implemented on DSP platform. Finally, the memristive chaotic system is applied to chaotic image encryption. The results of this study will be a guide to the application and instruction of memristors and memristive chaotic systems.

Keywords: Flux-Controlled, Memristor Model, Chaotic System, Attractor Coexistence, DSP Implementation, Image Encryption.

AMS Subject Classification: 68Q06, 68T99, 94C30, 94C60.

1. Introduction

In 1971, the author proposed memristor based on variable substitution [8]. Then, the authors proposed memristor devices and systems in 1976 [9]. The implementation of the memristor was reported by the HP Laboratories in 2008 [31]. The research results shocked the international electrical and electronic technology community, and made people interested in memristor research [14, 15]. The memristor as a memory element differs from the other three basic circuit elements in that it memorizes the quantity of the charge moving and its resistance is controlled through changes in current. It can lead to the construction of a series of novel chaotic circuit systems, which has become a topical issue in the research of nonlinear systems [7, 23, 33]. Meanwhile, research on the application of memristor in neural networks and secure communication has begun to flourish [1, 16], it is an important way for the future application of chaos theory. The memory properties of memristors have had a profound impact on neural networks, computer science, bioengineering, electronic engineering, secure communications, etc [11, 22, 26, 30].

The theory of chaos has flourished in recent decades. Throughout the history of chaos science, the early stage was mainly about the preliminary reveal of chaotic phenomenon, the establishment of chaotic system model and chaos theory. Early generation models of chaotic systems, such as Lorenz atmospheric turbulence equation, Chua's chaotic circuit, and Logistic insect population model, are generally derived from physical systems after simplification and abstraction [10, 21, 34]. The Rucklidge system, which was proposed in 1992, was originally used to study the two-dimensional convection of solutes, and it was observed to have chaotic phenomenon [29]. The Rucklidge system is a classic chaotic system, which has particularly sufficient dynamical behaviors, and has potential application prospects. Various properties of Rucklidge system have been analyzed in many fields such as Hopf bifurcation analysis, sliding mode control, synchronization and masking simulation [27, 35, 38]. Rucklidge chaotic systems based on

[1]School of Information Science and Engineering, Dalian Polytechnic University, Dalian, 116034, China
[2]Department of Mathematical Sciences, Giuseppe Luigi Lagrange, Politecnico di Torino, Corso Duca Degli Abruzzi 24, Torino, Italy
*Corresponding author: e-mail: moujun@csu.edu.cn, miaomiao@dlpu.edu.cn
Manuscript received 03 March 2023.

memristors are rarely studied. Memristive chaotic systems can produce complex nonlinear dynamical phenomena [6]. Different from the equilibrium points of general chaotic systems, the distribution of equilibrium points of memristive chaotic systems is a set of points located on a certain coordinate axis. Different equilibrium points make the chaotic oscillator system have two dynamical characteristics, stable and unstable [18, 20]. The trajectory of a general chaotic system is limited to a certain chaotic region [25]. In the memristive system, due to the different dynamical characteristics of the equilibrium point set, the system trajectory will be transferred to the periodic state from the chaotic state, and vice versa. Generally, an ideal chaotic system based on memristor is prone to generate infinite coexisting attractors, which can obtain multistability related to the initial value. Therefore, adding one or more memristors to the system can effectively observe the phenomenon of coexisting attractors [19, 24, 28].

In the existing articles related to flux-controlled memristors, there are not many types of flux-controlled memristor models used by researchers, basically the following: trigonometric function-based flux-controlled memristor model, hyperbolic function-based flux-controlled memristor model, absolute value function-based flux-controlled memristor model, and square function-based flux-controlled memristor model. The authors proposed a flux-controlled memristor described by a smooth quadratic nonlinear characteristic curve, and equivalent realized the function of the memristor by using resistors, capacitors, multipliers and operational amplifiers [2, 4]. A flux-controlled memristor described by smooth cubic nonlinear characteristic curves proposed in [3, 5]. The authors designed a general memristor simulator based on hyperbolic function [32]. Therefore, it is necessary to add new memristor models for further research of memory elements. In this paper, a novel smooth quartic nonlinear flux-controlled memristor model is proposed.

In order that the new flux-controlled memristor model must conform to the memristor characteristics and have good performance, we design a quartic function $q(\varphi)$, and add an absolute value function to the function species. The quartic function itself will be more sensitive to the change of the input than the square function, and after adding the absolute value function, the feedback of the output to the input is more complicated. And it is not like the trigonometric function as a periodic function, with the monotonic change of magnetic flux, charge is also continuously changing to new values. Compared to the above work, this has led to the design of a flux-controlled memristor that not only meets the characteristics of the memristor, but also has a faster response and greater amplitude of output variation. The circuit of memristive chaotic system is designed and simulated. This circuit is easy to integrate, and because of the simple fabrication process, it is ideal for mass production when a memristor is needed but no the circuit is easy to integrate. The application of chaotic systems in image encryption is currently a hot topic [12, 36]. Comparing with the previous encryption methods [13, 17, 37, 39], the system shows excellent performance in the application of image encryption, and also reflects the complexity of the memristive chaotic system.

In this paper, a new flux-controlled memristor model is designed and added it to the Rucklidge chaotic system. The other sections of this paper is organized as such: the memristor model and memristive chaotic system are described in Section 2. In Section 3, the dynamic properties of the system are given. The circuit implementation of the system is presented in Section 4. In Section 5, the system is applied to image encryption. Finally, the conclusions and results are provided in Section 6.

2. Chaotic system model with memristor

At present, the memristive chaotic system plays an important role in the research of chaos theory. In this section, a new memristor model and its circuit are designed. A memristive chaotic system is constructed based on it.

2.1. **The memristor model.** According to the theory of memristor, an ideal flux-controlled memristor model is given as

$$\begin{cases} i = W(\varphi)v, \\ \dfrac{d\varphi}{dt} = v, \end{cases}$$

where φ is the magnetic flux, i and v represent the current and voltage through the memristor; W(φ) is a nonlinear function of φ, called the memductance. The memristor model is equivalent to

$$q = f(\varphi).$$

Based on the above, a new smooth quartic nonlinear flux-controlled memristor model is designed as

$$q(\varphi) = k\varphi^2 + m\varphi^2\,|\varphi| + n\varphi^4,$$

where k, m, n are parameters. Set $\alpha = 2k$, $\beta = 3m$ and $\gamma = 4n$, the memductance is

$$W(\varphi) = \alpha\varphi + \beta\varphi\,|\varphi| + \gamma\varphi^3. \tag{1}$$

The characteristic curve of the memristor in φ-q plane and memductance relationship curve are shown in Fig.1. Condition of the passive flux-controlled memristor is that the instantaneous power consumed is non-negative. In Fig.1(b), the memductance is negative in a certain range, which means that the instantaneous power has a negative value, so this condition is not met. The memristor is active.

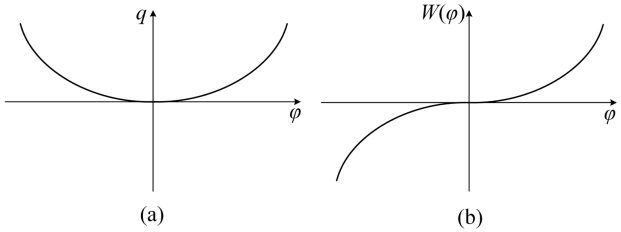


Figure 1. The characteristic curve of the memristor. (a) φ-q. (b) Memductance relationship curve.

According to the general definition of memristor, the quartic nonlinear flux-controlled memristor model is given as following

$$\begin{cases} i = W(\varphi)v, \\ \dfrac{d\varphi}{dt} = v, \\ W(\varphi) = \alpha\varphi + \beta\varphi\,|\varphi| + \gamma\varphi^3, \end{cases}$$

simulate the memristor model to examine its performance. A sinusoidal AC voltage source v=$Asin(2\pi Ft)$ is connected to the input of the memristor. The characteristics of the memristor are analyzed under different signal amplitude A and frequency F. Set parameters α=0.472, β=-1 and γ=0.472, the hysteresis loops of the memristor model at different A and F are plotted.

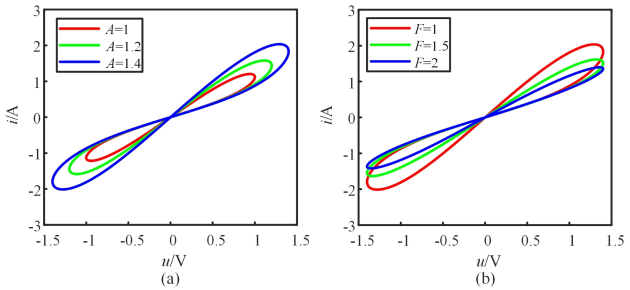


Figure 2. The pinched hysteresis loops of the memristor model at different A and F.
(a) F=1 and different A. (b) A=1.4 and different F.

Set A to 1, 1.2 and 1.4, and set F to 1, 1.5 and 2, respectively. The six "8"-shaped hysteresis loops passing through the zero point of the u-i plane are shown in Fig.2. Except for the origin, the $i(t)$ of the flux-controlled memristor model is a double-valued function of $v(t)$, and when the power frequency is the same, the increase of the voltage amplitude will lead to an increase in the side lobe area and a change in the shape. When the voltage amplitude is constant, as the frequency increases, the side lobe area gradually decreases and gradually approaches a straight line. Obviously, the designed mathematical model conforms to the three characteristics of memristor, which is a qualified memristor model.

The equivalent circuit of the memristor model is given in Fig.3, which includes 5 operational amplifiers, 4 multipliers, 13 resistors, 1 capacitor and 2 diodes.

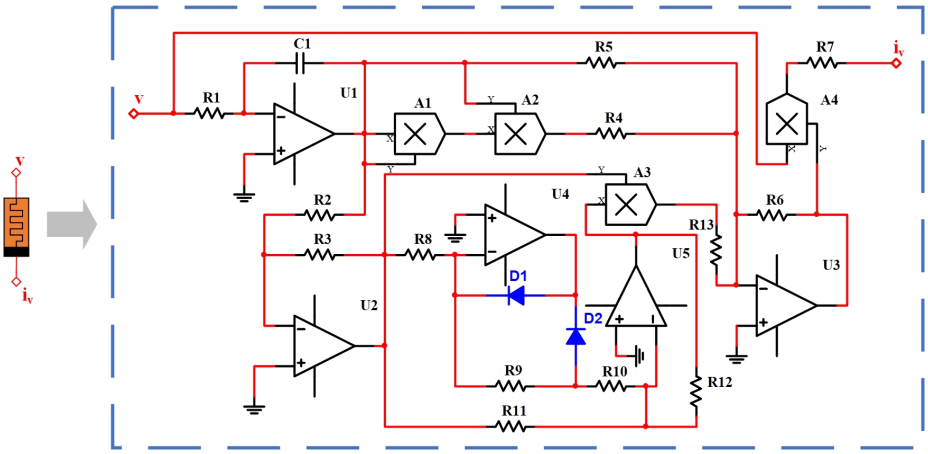


Figure 3. The equivalent circuit of the memristor model.

According to the basic principle of the circuit, the equivalent memductance is given as

$$W(\varphi) = \left(\frac{R_6}{R_5}\varphi - 0.1\frac{R_6}{R_{13}}\varphi\,|\varphi| + 0.01\frac{R_6}{R_4}\varphi^3 \right),$$

so

$$\alpha = \frac{R_6}{R_5}, \beta = -0.1\frac{R_6}{R_{13}}, \gamma = 0.01\frac{R_6}{R_4},$$

then the equivalent equation of the memristor is

$$\begin{cases} i_v = W(\varphi)v = \left(\dfrac{R_6}{R_5}\varphi - 0.1\dfrac{R_6}{R_13}\varphi\,|\varphi| + 0.01\dfrac{R_6}{R_4}\varphi^3 \right) v \\ \dfrac{d\varphi}{\mathrm{d}t} = -\dfrac{1}{R_1 C_1}v. \end{cases}$$

Set parameters α=0.472, β=-1, γ=0.472, the corresponding values of the equivalent circuit elements of the memristor model are provided in Table 1.

Table 1. Values of elements of the equivalent circuits in Fig.3.

Parameters	Elements	Values
R_1	Resistance	100KΩ
R_2, R_3, R_8, R_9, R_{11}, R_{12}	Resistance	10KΩ
R_4	Resistance	1.06KΩ
R_5	Resistance	106KΩ
R_6	Resistance	50KΩ
R_7	Resistance	2KΩ
R_{10}, R_{13}	Resistance	5KΩ
C_1	Capacitance	10nF
A_1-A_4	Multiplier	0.1

To verify that the equivalent circuit is correct in Multisim, set A=1 and F=1. The properties of the memristor model are presented in Fig.4. The result is as expected, proving that the equivalent circuit is correct. The active flux-controlled memristor model and equivalent circuit can be used in the study of chaotic systems and memristors.

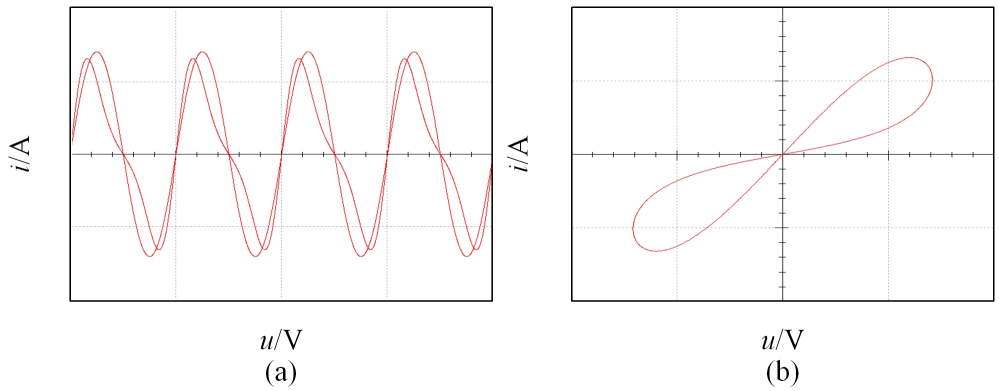


Figure 4. The time-domain waveform and volt-ampere characteristic curve implemented. (a) Time domain waveform. (b) Hysteresis loop.

2.2. **Model of the chaotic system.** A unified method was used to derive a 2D convection model with lateral constraints in the horizontal Boussinesq fluid layer. Convection in an applied horizontal or vertical magnetic field, convection in a layer of fluid rotating uniformly about a vertical axis, and thermal solute convection are analyzed separately. During the study, it was deduced that the convection in the horizontal magnetic field and the thermal solute convection have the same set of model equations, which show chaotic solutions and period-doubling cascades associated with Shil'nikov bifurcation. This is the first proof that the two-dimensional magnetic convection governing equation has chaotic solutions. The model is known as nonlinear convective Rucklidge chaotic system.

After removing all irrelevant constants in this 2D convection model, the equation can be written as

$$\ddot{y} - by = -a\dot{y} - yz, \dot{z} = -z + y^2.$$

The above equation can be expressed as a set of three coupled ODEs, which is the classical representation of the Rucklidge chaotic system as

$$\begin{cases} \dot{x} = -ax + by - yz, \\ \dot{y} = x, \\ \dot{z} = -z + y^2. \end{cases}$$

According to the mathematical model, the equivalent module circuit of the Rucklidge chaotic system is designed in Fig.5.

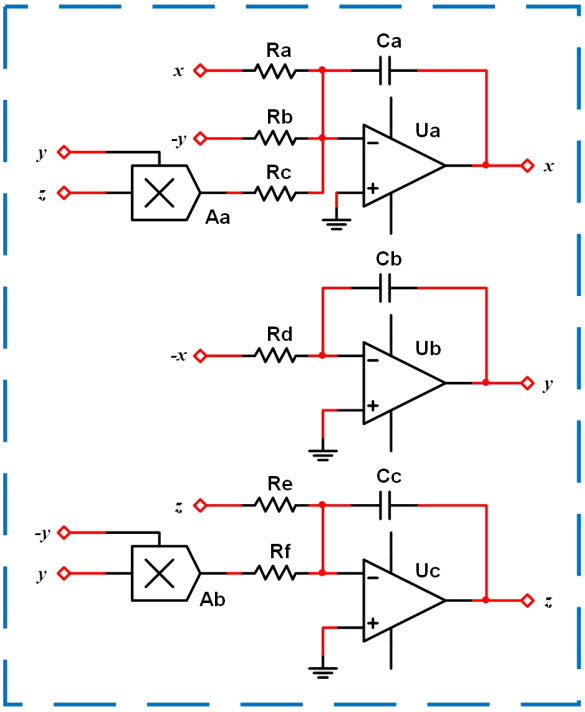


Figure 5. The equivalent module circuit of the Rucklidge system.

The new active flux-controlled memristor is introduced into the Rucklidge system to replace R_{d}, and the equivalent circuit of the memristive chaotic system is obtained in Fig.6.

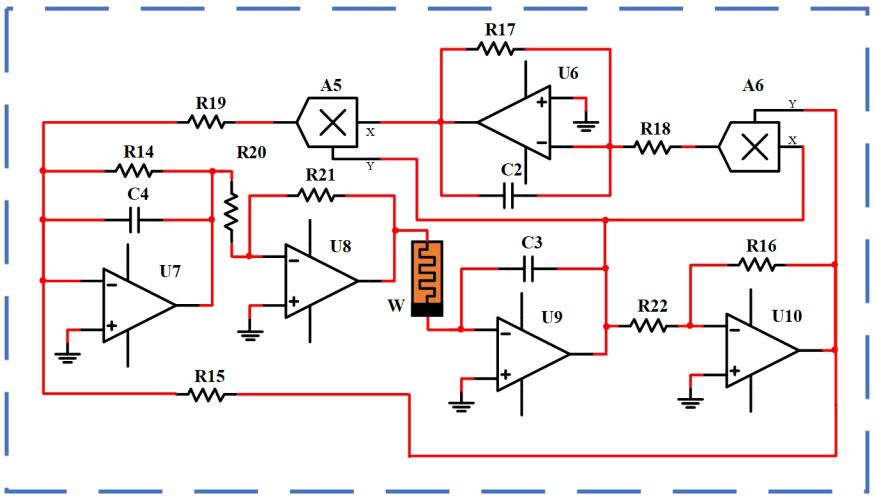


Figure 6. Equivalent circuit diagram of memristive chaotic system.

The equivalent circuit equation of the system is

$$\begin{cases} C_4\dfrac{\mathrm{d}V_x}{\mathrm{d}t} = -\dfrac{1}{R_{14}}V_x - \dfrac{1}{R_{15}}(-V_y) - \dfrac{1}{10R_{19}}V_yV_z, \\ C_3\dfrac{\mathrm{d}V_y}{\mathrm{d}t} = -\dfrac{1}{R_1}(-V_x)W(\varphi), \\ C_2\dfrac{\mathrm{d}V_z}{\mathrm{d}t} = -\dfrac{1}{R_{17}}V_z - \dfrac{1}{10R_{18}}V_y(-V_y), \\ C_1\dfrac{\mathrm{d}\varphi}{\mathrm{d}t} = -\dfrac{1}{R_1}(-V_x). \end{cases}$$

The model of the memristive chaotic system is

$$\begin{cases} \dot{x} = -ax + by - yz, \\ \dot{y} = x(cu + du\,|u| + eu^3), \\ \dot{z} = -z + y^2, \\ \dot{u} = x. \end{cases} \tag{2}$$

Analyze the memristive chaotic system and set a=1.65, b=3.48, c=0.472, d=-1, e=0.472, and the initial value is (1, 1, 1, 4). The Lyapunov exponent spectrum (LEs)is (0.2922, 0, -0.0158, -2.9351), and the Lyapunov dimension is 3.0942. It implies that the system is in chaos. The phase diagrams of the system are displayed in Fig.7.

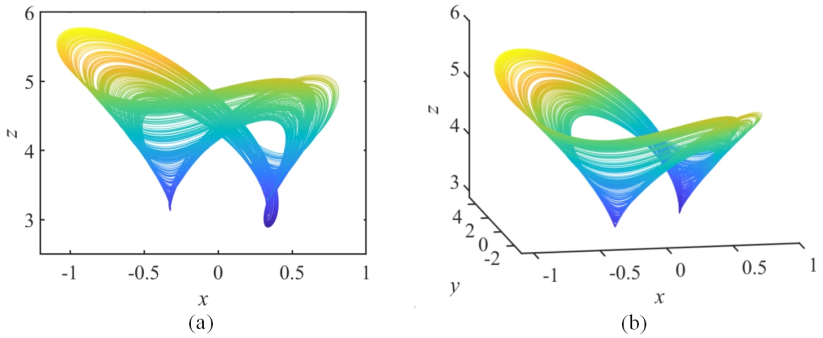


Figure 7. Phase diagrams of the system. (a) x-y. (b) x-y-z.

3. Dynamical analysis of the system

The availability of complex and rich dynamical behavior is an important criterion to measure whether a chaotic system is worthy of study. In this section, the dynamical behavior of the memristive chaotic system is studied by equilibrium points, bifurcations, LEs, and complexity to observe the special phenomena generated.

3.1. **Equilibrium analysis.** Observing the properties of equilibrium points is an important way to analyze the stability of chaotic systems. To calculate the equilibrium points, let us consider

$$\begin{cases} -ax + by - yz = 0, \\ x(cu + du\,|u| + eu^3) = 0, \\ -z + y^2 = 0, \\ x = 0. \end{cases}$$

The line equilibrium sets, $P_1(0,\ 0,\ 0,\ n)$ and $P_2(0,\ \pm b^{0.5},\ b,\ n)$ can be obtained, so the system has infinitely many equilibrium points. The Jacobi matrix J of the set of equilibrium points is given as

$$J = \begin{bmatrix} -a & b-z & -y & 0 \\ cu + du\,|u| + eu^3 & 0 & 0 & x(c + 2d\,|u| + 3eu^2) \\ 0 & 2y & -1 & 0 \\ 1 & 0 & 0 & 0 \end{bmatrix}.$$

The characteristic equation of P_1 is

$$f_1(\lambda) = -\lambda(\lambda + 1)(a_1\lambda^2 + a_2\lambda + a_3) = 0,$$

where a_1=-1, a_2=-a, a_3=ben^3+bdn^2+bcn and two non-zero eigenvalues in addition to -1. According to the Routh-Hurwitz criterion, the condition for the system to be balanced is that all coefficients satisfy a_1, a_2, a_3>0 and all roots lie in the left half-plane. The result is inconsistent with the stable condition, so P_1 is unstable, leading to unstable behavior of the system.

The characteristic equation of P_2 is

$$f_2(\lambda) = \lambda(b_1\lambda^3 + b_2\lambda^2 + b_3\lambda + b_4),$$

where b_1=1, b_2=a+1, b_3=a, b_4=2(en^3+dn^3+cn)b and three non-zero eigenvalues can be obtained. It means that the system is balanced when all coefficients are greater than 0 and $b_2b_3 > b_1b_4$. If this condition is satisfied, P_2 is stable; otherwise, P_2 is unstable.

3.2. **Bifurcation analysis.** Set b=3.48, c=0.472, d=-1, e=0.472, the initial value is (1, 1, 1, 4). When $a \in$(1.3, 6), the bifurcation diagram in Fig.8 shows that the system enters the chaotic state, goes through a short periodic window, then enters the chaotic state, and finally enters the periodic state through an anti-period-doubling bifurcation. This is consistent with changes in LEs.

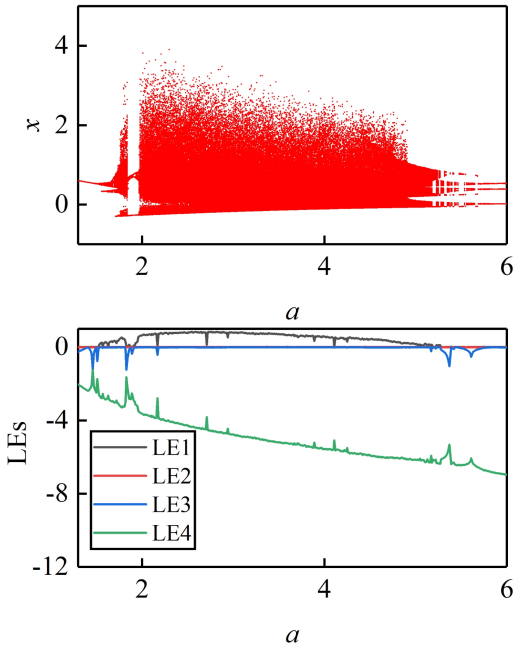


Figure 8. Bifurcation diagram and LEs of the system with a.

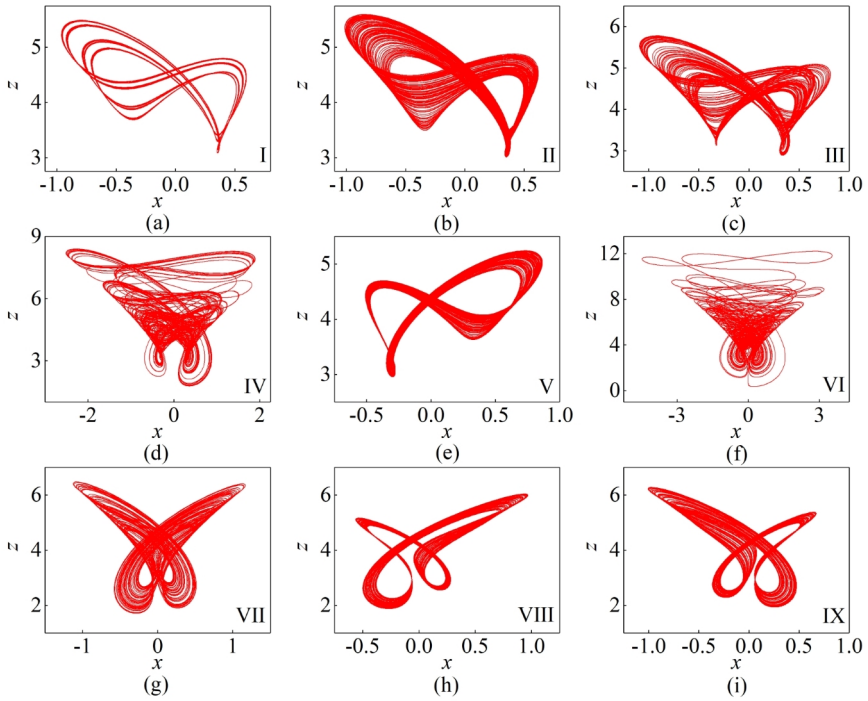


Figure 9. Chaotic attractors for different values of a. (a) Type-I for a=1.53. (b) Type-II for a=1.57. (c) Type-III for a=1.65. (d) Type-IV for a=1.75. (e) Type-V for a=1.93. (f) Type-VI for a=2.03. (g) Type-VII for a=4.77. (h) Type-VIII for a=5.05. (i) Type-IX for a=5.14.

Table 2. The Attractor states and Lyapunov exponent spectra corresponding to different values of a.

a	LEs	Attractor state
1.3-1.50	$(0, 0, -, -)$	quasi-periodic
1.51-1.56	$(+, 0, 0, -)$	Chaos I
1.57-1.64	$(+, 0, 0, -)$	Chaos II
1.65-1.73	$(+, 0, 0, -)$	Chaos III
1.74-1.81	$(+, 0, 0, -)$	Chaos IV
1.82-1.86	$(+, 0, -, -)$	Chaos IV
1.87	$(0, 0, 0, -)$	quasi-periodic
1.88-1.9	$(0, 0, -, -)$	quasi-periodic
1.91-1.93	$(+, 0, -, -)$	Chaos V
1.94-2.15	$(+, 0, 0, -)$	Chaos VI
2.16-2.18	$(+, 0, -, -)$	Chaos VI
2.19-4.10	$(+, 0, 0, -)$	Chaos VI
4.11	$(0, 0, -, -)$	quasi-periodic
4.12-4.68	$(+, 0, 0, -)$	Chaos VI
4.69-5.02	$(+, 0, 0, -)$	Chaos VII
5.03-5.12	$(+, 0, 0, -)$	Chaos VIII
5.13-5.15	$(+, 0, 0, -)$	Chaos IX
5.16-5.23	$(+, 0, -, -)$	Chaos IX
5.24-5.26	$(+, 0, 0, -)$	Chaos IX
5.27-5.38	$(0, 0, -, -)$	quasi-periodic
5.39	$(+, 0, 0, -)$	Chaos IX
5.40-5.43	$(0, 0, 0, -)$	quasi-periodic
5.44-5.83	$(0, 0, -, -)$	quasi-periodic
5.84-6	$(0, 0, 0, -)$	quasi-periodic

When the parameter a changes, nine different chaotic attractors could be found in the system, as shown in Fig.9. This phenomenon indicates that the system has excellent chaotic properties.

The range of the detailed evolution of the attractor, the corresponding LEs and the attractor states are shown in Table 2.

Set a=1.65, c=0.472, d=-1, e=0.472, the initial value is (1, 1, 1, 4). From the bifurcation diagram in Fig.10 at $c \in$(-1, 1.5), it can be seen that the system is in a chaotic state for a long time and then enters the periodic state. This is consistent with changes in LEs. Five types of chaotic attractors are observed as c changes, among which there is a new chaotic attractor, as shown in Fig.11. The range of the detailed evolution of the attractor, corresponding attractor states and LEs are shown in Table 3.

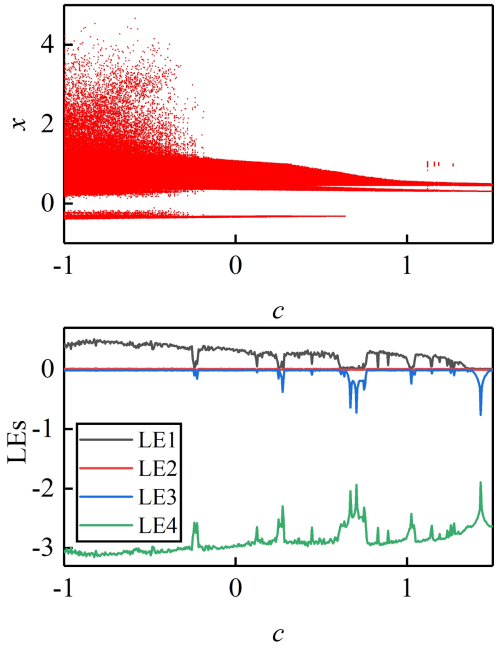


Figure 10. Bifurcation diagram and LEs of the system with c.

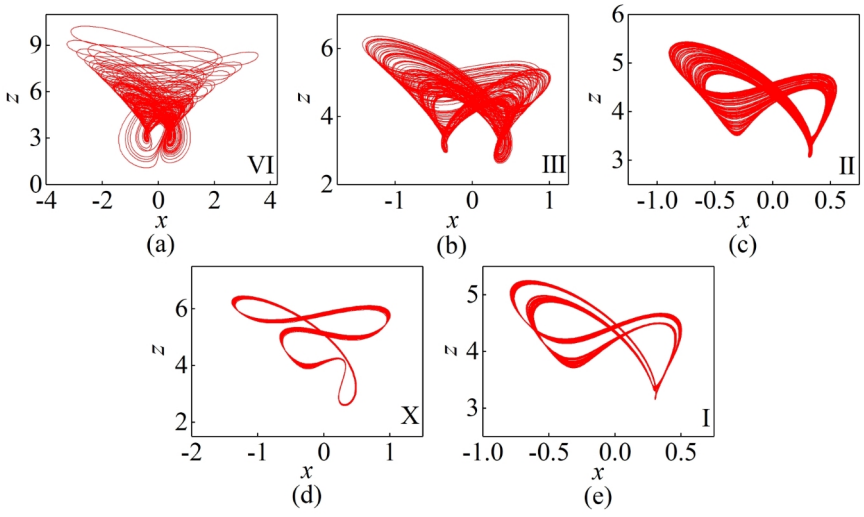


Figure 11. Chaotic attractors for different values of c. (a) Type-VI for c=-0.87. (b) Type-III for c=0.1. (c) Type-II for c=1. (d) Type-X for c=1.16. (e) Type-I for c=1.36.

Table 3. The attractor states and Lyapunov exponent spectra corresponding to different values of c.

c	LEs	Attractor state
−1-−0.28	$(+, 0, 0, -)$	Chaos VI
−0.27-−0.24	$(+, 0, 0, -)$	Chaos III
−0.23-−0.21	$(+, 0, -, -)$	Chaos III
−0.2-0.11	$(+, 0, 0, -)$	Chaos III
0.12	$(+, 0, -, -)$	Chaos III
0.13-0.25	$(+, 0, 0, -)$	Chaos III
0.26-0.28	$(+, 0, -, -)$	Chaos III
0.29-0.6	$(+, 0, 0, -)$	Chaos III
0.61-0.74	$(+, 0, -, -)$	Chaos III
0.75-0.77	$(+, 0, -, -)$	Chaos II
0.78-1.02	$(+, 0, 0, -)$	Chaos II
1.03-1.06	$(+, 0, -, -)$	Chaos II
1.07-1.13	$(+, 0, 0, -)$	Chaos II
1.14	$(+, 0, -, -)$	Chaos II
1.15	$(+, 0, 0, -)$	Chaos II
1.16	$(+, 0, 0, -)$	Chaos X
1.17-1.24	$(+, 0, 0, -)$	Chaos II
1.25	$(+, 0, -, -)$	Chaos I
1.26	$(+, 0, 0, -)$	Chaos I
1.27	$(+, 0, -, -)$	Chaos X
1.28-1.34	$(+, 0, 0, -)$	Chaos I
1.35-1.37	$(0, 0, 0, -)$	quasi-periodic
1.38-1.47	$(0, 0, -, -)$	quasi-periodic
1.48-1.5	$(0, 0, 0, -)$	quasi-periodic

3.3. **Multistability analysis.** Multistability is a particular state in chaotic systems, often referred to as attractors coexistence.

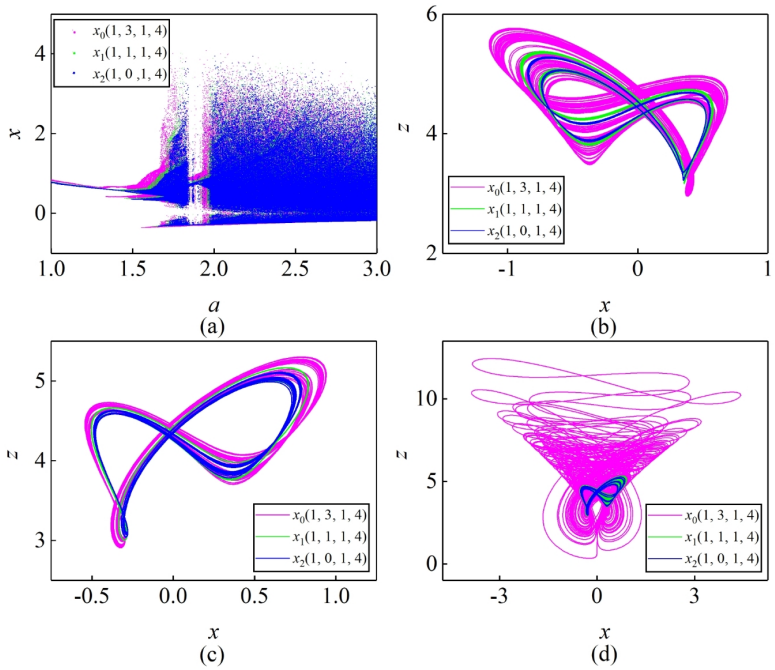


Figure 12. Attractor coexistence with respect to parameter a. (a) Bifurcation diagram with initial values (1, 3, 1, 4)(pink points) , (1, 1, 1, 4)(green points) and (1, 0, 1, 4)(blue points). (b) Attractor coexistence for a=1.5. (c) Attractor coexistence for a=1.9. (d) Attractor coexistence for a=1.96.

The system has infinitely many equilibrium points, leading to the possibility of multiple coexisting solutions. The diagram of coexistence bifurcation is generally applied to study the coexistence of attractors. Set b=3.48, c=0.472, d=-1, e=0.472, with (1, 3, 1, 4), (1, 1, 1, 4) and (1, 0, 1, 4) as the initial value, the diagram of coexistence bifurcation is obtained in Fig.12(a). The chaotic range of the system is obviously different under the three initial values. As a increases, the states of the three bifurcations change sequentially. To observe this phenomenon clearly, several typical coexistence of attractors are displayed in Fig.12. The coexistence of chaotic attractors and periodic attractors are shown in Fig.12(b) and (c). The coexistence of different types of chaotic attractors is shown in Fig.12(d).

As above, the variation of the initial value also has attractors coexistence for the same parameter b. From the bifurcation diagram in Fig.13(a), it is observed that the chaotic performance of the system is different at the three initial values. When the initial value is (1, 3, 1, 4), the system has better chaotic performance in $c \in (0, 1.5)$ and enters the periodic state slower. The coexistence of Chaos II and III is shown in Fig.13(b). The coexistence of Chaos I and II is shown in Fig.13(c). The coexistence of two periodic attractors and chaotic attractor is shown in Fig.13(d). The coexistence analysis of attractors of parameters a and c shows that the memristive chaotic system has high complexity.

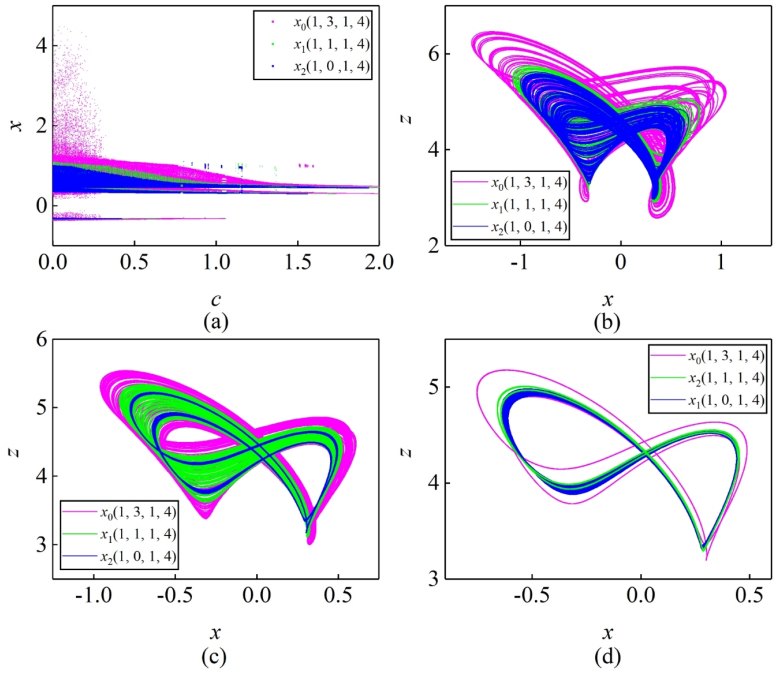


Figure 13. Attractor coexistence with respect to parameter c. (a) Bifurcation diagram with initial values (1, 3, 1, 4)(pink points) , (1, 1, 1, 4)(green points) and (1, 0, 1, 4)(blue points). (b) Attractor coexistence for c=0.5. (c) Attractor coexistence for c=1. (d) Attractor coexistence for c=1.9.

3.4. **State transition.** There is a state transition phenomenon in the system, which is expressed as the transition between the chaotic state and the periodic state in the iterative sequence, which reflects the complex dynamical characteristics. Set a=1.87, b=3.48, c=1, d=-1, e=0.472, the initial value is (1, 1, 4, 4), the iterative sequence in Fig.14(a) begins to observe a short-term chaotic state, and then degenerates into a periodic state. The iterative sequence of the periodic state is shown in Fig.14(b). The chaotic attractor at the beginning of the iterative sequence is presented in Fig.14(c), and the phase diagram of the periodic attractor after degradation is given in Fig.14(d).

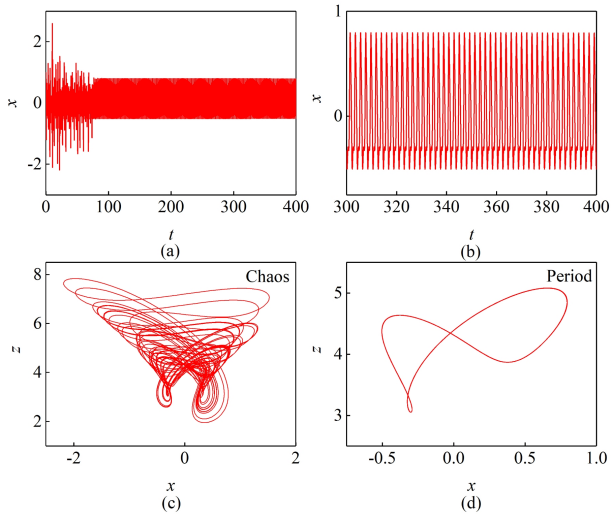


Figure 14. Iterative sequences and attracters (x-z) for chaotic degradation. (a) Iterative sequence for $t \in(0, 400)$. (b) Iterative sequence for $t \in(300, 400)$. (c) Chaotic attractor. (d) Periodic attractor.

3.5. **SE complexity.** The complexity analysis is a useful tool to reflect the correlation between a sequence and a random sequence. In this case, the SE algorithm to reflect the complexity of the system is used. Set c=0.472, d=-1, e=0.472, the initial value is (1, 1, 1, 4), and the SE complexity (a-b) is shown in Fig.15(a). Set b=3.48, d=-1, e=0.472, the initial value unchanged, and the SE complexity (a-c) is given in Fig.15(b). The SE complexity of the system is low when it is in a periodic state and high when it is in a chaotic state.

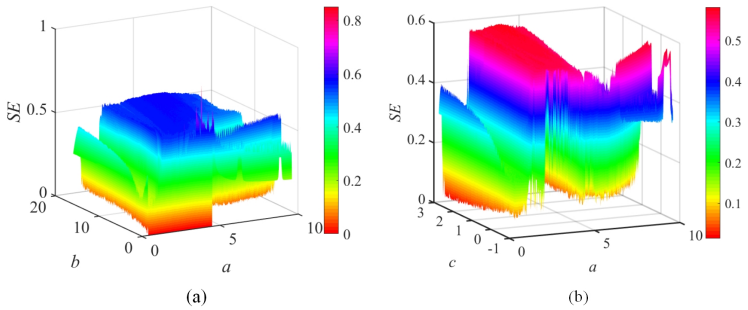


Figure 15. 3D SE complexity for different parameters. (a) $a \in(0.3, 9.7)$, $b \in(0, 17)$. (b) $a \in(0.3, 9.7)$, $c \in(-1, 3)$.

4. Circuit simulation and DSP implementation

This section discusses the implications of the system for the application and verifies its dynamical properties. It proceeds in two ways, the first is to use the Multisim software to simulate the equivalent circuit, and then the system is implemented with DSP.

4.1. **Analog circuit simulation.** Simulate this memristive chaotic system in Multisim to check the performance of the designed equivalent circuit. According to the parameters set in the system, a=1.65, b=3.48, c=0.472, d=-1, e=0.472, the initial condition is (1, 1, 1, 4), the corresponding circuit element values are shown in Table 4. Check the correctness of the analog circuit by changing the parameter a. When a is 0.5, 1.5, 1.56, and 2, the corresponding R_{14} is 200KΩ, 67KΩ, 64KΩ and 50KΩ.

Table 4. The attractor states and Lyapunov exponent spectra corresponding to different values of c.

Parameters	Elements	Values
R_1, R_{17}	Resistance	100KΩ
R_2, R_3, R_8, R_9, R_{11}, R_{12} R_{16}, R_{18}-R_{22}	Resistance	10KΩ
R_4	Resistance	1.06KΩ
R_5	Resistance	106KΩ
R_6	Resistance	50KΩ
R_7	Resistance	2KΩ
R_{10}, R_{13}	Resistance	5KΩ
R_{14}	Resistance	60KΩ
R_{15}	Resistance	29KΩ
C_1-C_4	Capacitance	10nF
A_1-A_6	Multiplier	0.1

The results are presented in Fig.16(a), (d), (g) and (j). The attractors observed conform to the results of the numerical simulations in Matlab, indicating that the circuit design is correct. The equivalent circuit can be used in physical applications.

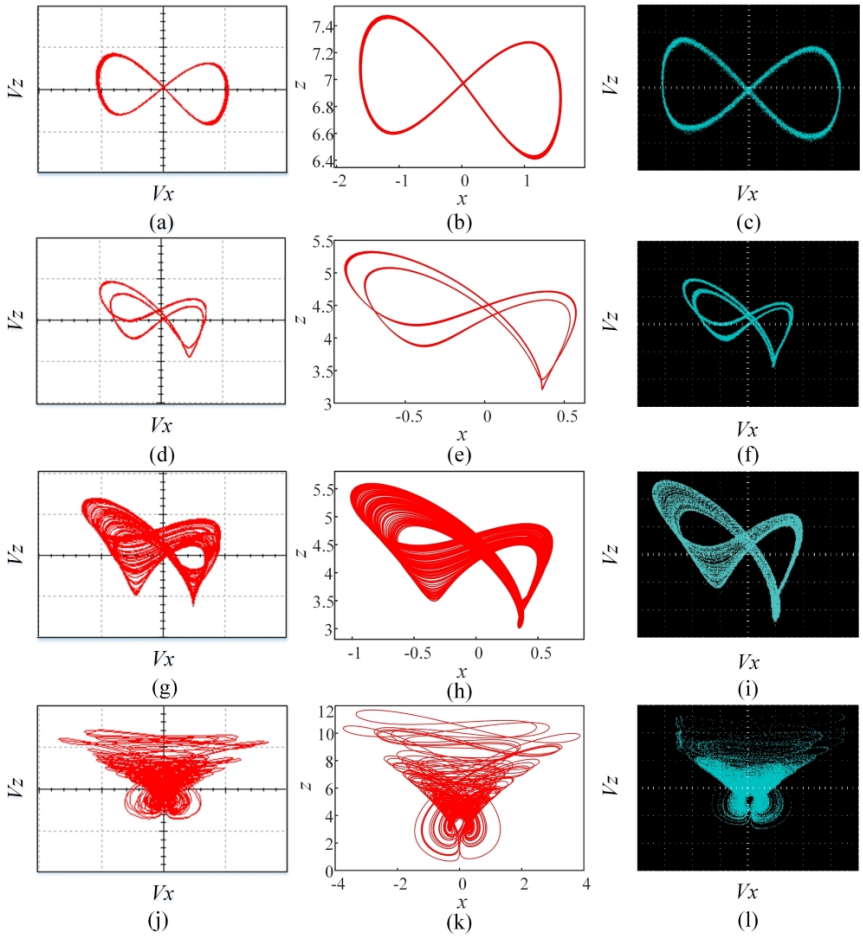


Figure 16. Comparison of attractors (V_x-V_z) obtained by Multisim and DSP and attractors (x-z) simulated by Matlab. (a) Attractor with R_{14}=200KΩ in Multisim. (b) Attractor with a=0.5 in Matlab. (c) Attractor with a=0.5 in DSP. (d) Attractor with R_{14}=67KΩ in Multisim. (e) Attractor with a=1.5 in Matlab. (f) Attractor with a=1.5 in DSP. (g) Attractor with R_{14}=64KΩ in Multisim. (h) Attractor with a=1.56 in Matlab. (i) Attractor with a=1.56 in DSP. (j) Attractor with R_{14}=50KΩ in Multisim. (k) Attractor with a=2 in Matlab. (l) Attractor with a=2 in DSP.

4.2. **DSP implementation.** DSP chips are widely used in digital control and motion control. According to different needs, they can perform operations at a higher speed. To run the system on the DSP chip unnecessary check and observe the results. The design of the hardware block diagram is given in Fig.17.



Figure 17. DSP software implementation flowchart.

The chaotic sequences of the system are transformed into analog signals by the DSP platform, and then the attractor phase diagram is displayed by an oscilloscope. The DSP program flow is shown in Fig.18.

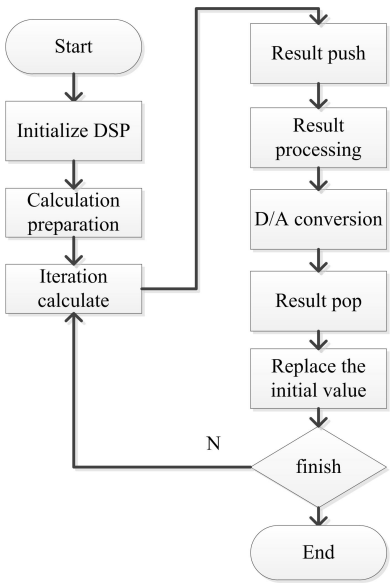


Figure 18. DSP software implementation flowchart.

The DSP operating platform of the system is presented in Fig.19.

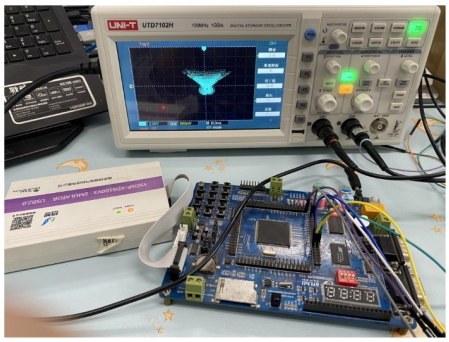


Figure 19. DSP hardware implementation platform.

Set b=3.48, c=0.472, d=-1, e=0.472, the initial value is set to (1, 1, 1, 4), and the attractors on the oscilloscope are shown in Fig.16(c), (f), (i) and (l). Obviously, the simulation results on the DSP are exactly corresponding. The realization on the platform of DSP proves the feasibility in physical application.

5. Application in image encryption

Image encryption based on chaotic system is a hot research topic recently. Memristive chaotic systems have complex dynamical characteristics and have greater application prospects in image encryption research. In this section, an image encryption scheme for memristive chaotic system based on smooth quartic nonlinear flux-controlled memristor is proposed to verify its advantages in image encryption.

5.1. **Description of the encryption process.** The architecture of the image encryption scheme based on amnestic chaos system consists of four main modules: chaotic sequence generator, Arnold permutation and DNA triplet mutation, as shown in Fig.20. The specific process of encryption and decryption is completed by four steps.

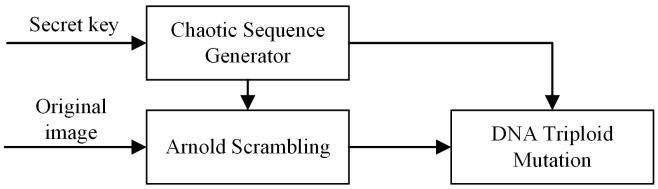


Figure 20. The architecture of the image encryption scheme based on memristive chaotic system.

Table 5. DNA triploid mutation ruler.

Ruler	1	2	3	4	5	6	7	8
A	A	A	U	U	G	G	C	C
T	C	G	C	G	U	A	U	A
C	G	C	G	C	A	U	A	U
G	U	U	A	A	C	C	G	G

(1) Set the initial value, parameters, time step and discarded number N_0 of the memristive chaotic system. By iterating this system, three discrete chaotic sequences ($x(i)$, $y(i)$, $z(i)$) are obtained, which have the same length as the original image. The operation is performed on the three sequences as

$$k(i) = \mathrm{mod}(\mathrm{ceil}(((x(i) + y(i) + z(i))/3) * 10^8), 256),$$

where the ceil(x) means that the value of x is reduced to the value with decimal places removed.

(2) Arnold permutation is first introduced to obtain the permuted image S1, and then the pixel substitution operation is implemented based on the DNA mutation rules κ in Table 5 as

$$\begin{cases} \mathrm{S2}(i) = f(\mathrm{S1}(i), \kappa(i)), \\ \kappa(i) = \mathrm{mod}(k(i), 8) + 1, \end{cases}$$

where $f(x(i), y(i))$ represents DNA triploid mutation function.

(3) The image decryption process operates in the reverse steps of encryption.

5.2. **Analysis of simulation results.** The initial values of the memristive chaotic system are set to (1, 1, 1, 4) and the parameters are set to a=1.65, b=3.48, c=0.472, d=-1, e=0.472.

The standard grayscale images of size 256×256 Lena, fruits, camera are selected, and the experimental results are shown in Fig.21.

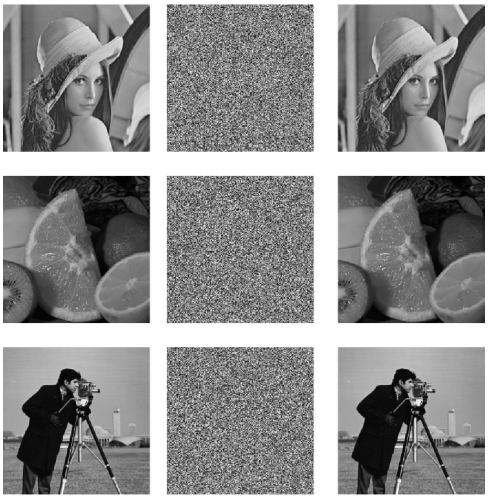


Figure 21. Encryption and decryption testing. (a) The plaintext images in first column. (b) The ciphertext images in second column. (c) The decrypted images in the third column.

5.3. **Histogram analysis.** Histogram analysis is a common method for analyzing statistical information of images. The more uniform the distribution of the image histogram after encryption, the better the effect of image encryption. The grayscale histogram changes of Lena's image before and after encryption are shown in Fig.22.

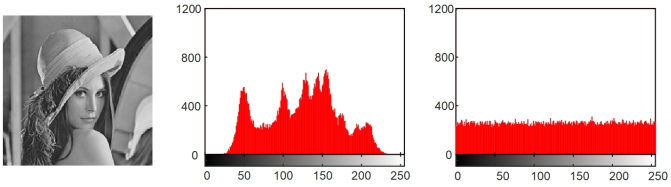


Figure 22. Histogram analysis. (a) Lena image. (b) Histogram of Lena plaintext image. (c) Histogram of Lena ciphertext image.

It can be seen that the histogram of the encrypted Lena image is evenly distributed without significant features. The performance of this encryption algorithm is strong from the above.

5.4. **Correlation analysis.** 3000 pairs of pixel points are selected randomly and are used to perform correlation tests in the horizontal, the vertical and diagonal directions of the image. The correlation coefficient r_{xy} is given by

$$r_{xy} = \frac{\operatorname{cov}(x,y)}{\sqrt{D(x)D(y)}},$$

where

$$\begin{cases} E(x) = \dfrac{1}{N}\displaystyle\sum_{i=1}^{N} x_i, \\ D(x) = \dfrac{1}{N}\displaystyle\sum_{i=1}^{N} [x_i - E(x)]^2, \\ \operatorname{cov}(x,y) = E\left\{[x - E(x)]\,[y - E(y)]\right\}. \end{cases}$$

The correlation coefficient of the Lean image is listed in Table 6.

Table 6. Correlation analysis of encryption scheme based on the memristive chaotic system.

Direction	Image type	Correlation coefficient (original image)	Correlation coefficient (encrypted image)
Level	Lena	0.9692	−0.0010
Vertical	Lena	0.9423	−0.0067
Diagonal	Lena	0.9160	0.0040

5.5. **Entropy analysis.** The information entropy is a major indicator of the randomness of information. The information entropy of the encrypted image is closer to 8, which means the more random the distribution of its pixel value is, the better the encryption effect is. The information entropy is defined as

$$H(m) = \sum_{i=0}^{L-1} P(m_i) \log \frac{1}{P(m_i)},$$

where L represents the number of pixel types, m is the pixel type, and P is the probability of the pixel type. In this encryption scheme L=256, m_i ∈(0, 1, 2, ..., 255), $P(m_i)$ ∈[0, 1] and $\sum_i P(m_i) = 1$. The calculation results is shown in Table 7. Compared with previous studies, it shows that the algorithm can effectively improve the information entropy.

Table 7. Performance comparison of encryption schemes based on different chaotic systems.

Refs	Image type	System type	Entropy
[26]	Lena	Multi-scroll chaotic system	7.9889
[27]	Lena	Multi-wing chaotic system	7.9974
[28]	Lena	Multi-scroll chaotic system	7.9975
[29]	Lena	Multi-wing chaotic system	7.9976
This work	Lena	Flux-controlled memristive chaotic system	7.9978

5.6. **Sensitivity analysis.** The key sensitivity analysis means that a small change in the key will eventually lead to a significant change in the ciphertext. The security of chaotic encryption lies in its initial value sensitivity, which means that cracking with a value close to the initial value will not recover the original image. The sensitivity test keys are (x_1, y_1, z_1), and the key sensitivity test results with a key change of 10^{-15} are shown in Fig.23. And the differential image is used to verify the initial value sensitivity. It can be seen that the encrypted image after a slight modification of the key parameter value is very different from the correct encrypted image, indicating that the encryption system has strong robustness.

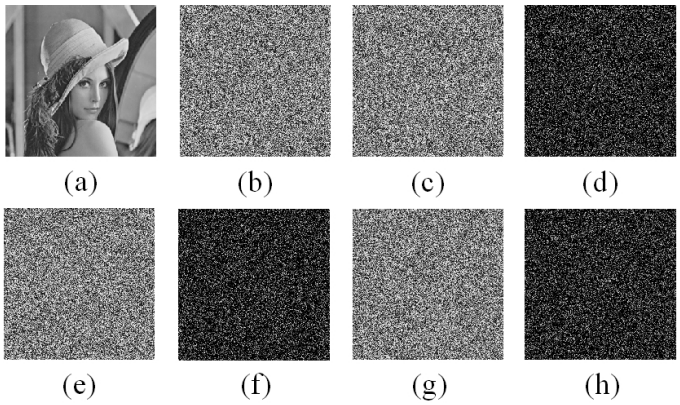


Figure 23. Key sensitivity test. (a) Lena image. (b) Ciphertext image with correct key. (c) Ciphertext image when x_1=x_1+10^{-15}. (d) differential image between (b) and (c). (e) Ciphertext image when y_1=y_1+10^{-15} (f) differential image between (b) and (e). (g) Ciphertext image when z_1=z_1+10^{-15}. (h) differential image between (b) and (g).

6. Conclusion

In this paper, a new active quartic nonlinear flux-controlled memristor model with superior performance is proposed. Thereafter, the memristive chaotic system is constructed based on this memristor and its complex and rich dynamical behaviors, including attractor coexistence phenomenon and state transfer phenomenon, are shown by analyzing the bifurcation diagrams, Lyapunov exponential spectrum, multistability, and SE complexity of the system. Moreover, the designed memristor model and memristive chaotic system are verified by equivalent circuit simulation on Multisim and implementation on DSP, showing the feasibility of their physical applications. Finally, the experimental results show that the image encryption scheme based on the flux-controlled memristive chaotic system has better security performance. The study is contributive to the design and application of the memristor model. The research of neural network is hot at present, and we will try the coupling of this memristor with neuron in the next step. In addition, the memcapacitor and meminductor can be studied by referring to the design process of the memristor.

7. Acknowledgment

This work was supported by the National Natural Science Foundation of China (Grant Nos. 62061014); The Natural Science Foundation of Liaoning province (2020-MS-274); The Basic Scientific Research Projects of Colleges and Universities of Liaoning Province (Grant Nos. LJKZ0545).

References

[1] Adhikari, S.P., Yang, C., Kim, H., Chua, L.O. Memristor bridge synapse-based neural network and its learning, *IEEE Transactions on Neural Networks and Learning Systems*, V.23, N.9, 2012, pp.1426-1435.

[2] Bao, B., Jian-Ping, X., Zhong, L. Initial state dependent dynamical behaviors in a memristor based chaotic circuit, *Chinese Physics Letters*, V.27, N.7, 2010, p.070504.

[3] Bao, B., Liu, Z. Xu, J. Steady periodic memristor oscillator with transient chaotic behaviours, *Electronics Letters*, V.46, N.3, 2010, p.228.

[4] Bao, B., Xu, J.-P., Zhou, G.-H., Ma, Z.-H., Zou, L. Chaotic memristive circuit: Equivalent circuit realization and dynamical analysis, *Chinese Physics B*, V.20, N.12, 2011, p.120502.

[5] Bao, B., Zhong, L., Jian-Ping, X. Transient chaos in smooth memristor oscillator, *Chinese Physics B*, V.19, N.3, 2010, p.030510.

[6] Cafagna D., Grassi, G. On the simplest fractional-order memristor-based chaotic system, *Nonlinear Dynamics*, V.70, N.2, 2012, pp.1185-1197.

[7] Chen, Y., Mou, J., Jahanshahi, H., Wang, Z., Cao, Y. A new mix chaotic circuit based on memristor-memcapacitor, *The European Physical Journal Plus*, V.138, N.1, 2023, p.78.

[8] Chua, L. Memristor-the missing circuit element, *IEEE Transactions on Circuit Theory*, V.18, N.5, 1971, pp.507-519.

[9] Chua, L.O., Kang, S.M. Memristive devices and systems, *Proceedings of the IEEE*, V.64, N.2, 1976, pp.209-223.

[10] Chua, L.O., Itoh, M., Kocarev, L., Eckert, K. Chaos synchronization in Chua's circuit, *Journal of Circuits, Systems, and Computers*, V.3, N.01, 1993, pp.93-108.

[11] Gao, X., Mou, J., Banerjee, S., Zhang, Y. Color-gray multi-image hybrid compression-encryption scheme based on BP neural network and knight tour, *IEEE Transactions on Cybernetics*, V.53, N.8, 2023, pp.5037-5047.

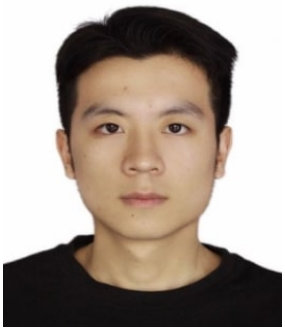
[12] Gao, X., Sun, B., Cao, Y., Banerjee, S., Mou, J. A color image encryption algorithm based on hyperchaotic map and DNA mutation, *Chinese Physics B*, V.32, N.3, 2023, p.030501.

[13] Hong, Q., Li, Y., Wang, X., Zeng, Z. A versatile pulse control method to generate arbitrary multidirection multibutterfly chaotic attractors, *IEEE Transactions on Computer-Aided Design of Integrated Circuits and Systems*, V.38, N.8, 2019, pp.1480-1492.

[14] Kim, H., Sah, M.P., Yang, C., Cho, S., Chua, L.O. Memristor emulator for memristor circuit applications, *IEEE Transactions on Circuits and Systems I: Regular Papers*, V.59, N.10, 2012, pp.2422-2431.

[15] Kvatinsky, S., Friedman, E.G., Kolodny, A., Weiser, U.C. TEAM: Threshold adaptive memristor model, *IEEE Transactions on Circuits and Dystems I: Regular Papers*, V.60, N.1, 2012, pp.211-221.

[16] Lin, H., Wang, C., Hong, Q., Sun, Y. A multi-stable memristor and its application in a neural network, *IEEE Transactions on Circuits and Systems II: Express Briefs*, V.67, N.12, 2020, pp.3472-3476.
[17] Lin, H., Wang, C., Yu, F., Xu, C., Hong, Q., Yao, W., Sun, Y. An extremely simple multiwing chaotic system: dynamics analysis, encryption application, and hardware implementation, *IEEE Transactions on Industrial Electronics*, V.68, N.12, 2020, pp.12708-12719.
[18] Liu, X., Mou, J.,Yan, H., Bi, X. Memcapacitor-coupled chebyshev hyperchaotic map, *International Journal of Bifurcation and Chaos*, V.32, N.12, 2022, p.2250180.
[19] Liu, X., Mou, J., Wang, J., Banerjee, S., Li, P. Dynamical analysis of a novel fractional-order chaotic system based on memcapacitor and meminductor, *Fractal and Fractional*, V.6, N.11, 2022, p.671.
[20] Liu, X., Mou, J., Zhang, Y., Cao, Y. A new hyperchaotic map based on discrete memristor and meminductor: dynamics analysis, encryption application, and DSP implementation, *IEEE Transactions on Industrial Electronics*, 2023.
[21] Logan, J., Allen, J. Nonlinear dynamics and chaos in insect populations, *Annual Review of Entomology*, V.37, N.1, 1992, pp.455-477.
[22] Ma, T., Mou, J., Li, B., Banerjee, S., Yan, H. Study on the complex dynamical behavior of the fractional-order hopfield neural network system and its implementation, *Fractal and Fractional*, V.6, N.11, 2022, p.637.
[23] Ma, X., Mou, J., Liu, J., Ma, C., Yang, F., Zhao, X. A novel simple chaotic circuit based on memristor-memcapacitor, *Nonlinear Dynamics*, V.100, N.3, 2020, pp.2859-2876.
[24] Ma, Y., Mou, J., Lu, J., Banerjee, S., Cao, Y. A discrete memristor coupled two-dimensional generalized square hyperchaotic maps, *Fractals*, 2023.
[25] Ma, Y., Mou, J., Jahanshahi, H., Alkhateeb, A.F., Bi, X. Design and DSP implementation of a hyperchaotic map with infinite coexisting attractors and intermittent chaos based on a novel locally active memcapacitor, *Chaos, Solitons & Fractals*, V.173, 2023, p.113708.
[26] Ma, T., Mou, J., Yan, H., Cao, Y. A new class of Hopfield neural network with double memristive synapses and its DSP implementation, *The European Physical Journal Plus*, V.137, N.10, 2022, pp.1-19.
[27] Pehlivan, I., Uyarolu, Y., Youn, M. Chaotic oscillator design and realizations of the Rucklidge attractor and its synchronization and masking simulations, *Scientific Research and Essays*, V.5, N.16, 2010, pp.2210-2219.
[28] Ren, L., Mou, J., Banerjee, S., Zhang, Y. A hyperchaotic map with a new discrete memristor model: Design, dynamical analysis, implementation and application, *Chaos, Solitons & Fractals*, V.167, 2023, p.113024.
[29] Rucklidge, A.M. Chaos in models of double convection, *Journal of Fluid Mechanics*, V.237, 1992, pp.209-229.
[30] Sha, Y., Mou, J., Banerjee, S., Zhang, Y. Exploiting flexible and secure cryptographic technique for multi-dimensional image based on graph data structure and three-input majority gate, *IEEE Transactions on Cybernetics*, 2023.
[31] Strukov, D.B., Snider, G.S., Stewart, D.R., Williams, R.S. The missing memristor found, *Nature*, V.453, N.7191, 2008, pp.80-83.
[32] Sun, J., Yang, J., Liu, P. Design of general flux-controlled and charge-controlled memristor emulators based on hyperbolic functions, *IEEE Transactions on Computer-Aided Design of Integrated Circuits and Systems*, V.42, N.3, 2022, pp.956-967.
[33] Sun, J., Zhao, X., Fang, J., Wang, Y. Autonomous memristor chaotic systems of infinite chaotic attractors and circuitry realization, *Nonlinear Dynamics*, V.94, N.4, 2018, pp.2879-2887.
[34] Tucker, W. The Lorenz attractor exists, *Comptes Rendus de l'Académie des Sciences-Series I-Mathematics*, V.328, N.12, 1999, pp.1197-1202.
[35] Vaidyanathan, S. Global chaos synchronization of Rucklidge chaotic systems for double convection via sliding mode control, *International Journal of ChemTech Research*, V.8, N.8, 2015, pp.61-72.
[36] Wang, L., Cao, Y., Jahanshahi, H., Wang, Z., Mou, J. Color image encryption algorithm based on Double layer Josephus scramble and laser chaotic system, *Optik*, V.275, 2023, p. 170590.
[37] Wang, N., Li, C., Bao, H., Chen, M., Bao, B. Generating multiScroll chua's attractors via simplified piecewise-linear Chua's diode, *IEEE Transactions on Circuits and Systems I: Regular Papers*, V.66, N.12, 2019, pp.4767-4779.
[38] Wang, X. Si'lnikov chaos and Hopf bifurcation analysis of Rucklidge system, *Chaos, Solitons & Fractals*, V.42, N.4, 2009, pp.2208-2217.
[39] Wang, T., Song, L., Wang, M., Zhuang, Z. A novel image encryption algorithm based on parameter-control scroll chaotic attractors, *IEEE Access*, V.8, 2020, pp.36281-36292.



Yanjie Ma - received the B.Sc. degree from Dalian Polytechnic University, Dalian, China. He is currently pursuing the Ph.D. degree in Control Science and Engineering at the same University. His mainly research interest includes chaos theory and application.



Jun Mou - received the B.Sc., M.Sc. and Ph.D. degrees in Physics and Electronics from Central South University, Changsha, China. He is currently a Professor at the School of Information Science and Engineering, Dalian Polytechnic University, China. His mainly research interest includes the nonlinear system control, secure communication, power system automation and smart grid research. He is Associate Editors of two journals of MDPI.



Santo Banerjee - was working as Associate Professor, in the Institute for Mathematical Research (INSPEM), University Putra Malaysia, till 2020, and also a founder member of the Malaysia-Italy Centre of Excellence in Mathematical Science, UPM, Malaysia. He is now associated with the Department of Mathematics, Politecnico di Torino, Italy. His research is mainly concerned with nonlinear dynamics, chaos, complexity and secure communication.



Miao Miao - received M.Sc. degree from Dalian Polytechnic University. She is working in the School of Information Science and Engineering of the same university. Her mainly research interest includes chaos theory and applications.